17.0 DEVELOPMENT OF ADVANCED NICKEL-TITANIUM-HAFNIUM ALLOYS FOR TRIBOLOGY APPLICATIONS

Sean Mills (Mines)
Faculty: Aaron Stebner and Mike Kaufman (Mines)
Industrial Mentors: Chris Dellacorte and Ron Noebe (NASA GRC)

17.1 Project Overview and Industrial Relevance

This project initiated in Fall 2015 and is supported by CANFSA. The research performed during this project will serve as the basis for a Ph.D. thesis program for Sean Mills.

The high hardness, high compressive elastic strength, and good corrosion resistance of ternary Ni-Ti-Hf alloys makes them optimum candidates for specialized bearing applications. In addition, aged Ni-Ti-Hf alloys exhibit superelastic hysteresis curves under compressive loading, which results in a nearly doubled toughness compared to conventional binary Ni-Ti (**Figure 17.1**). Conventional superelastic Ni-Ti alloys are known to experience high hardness and high residual stresses upon rapid quenching, resulting in cracking and machining distortion, whereas secondary precipitates can over-coarsen if cooled slowly, thereby reducing the material hardness. This project is designed to elucidate the effects of hafnium additions on the structure and properties of Ni-Ti-Hf alloys, with an emphasis on bearing element performance. It will be shown that hafnium additions have a significant impact on the transformation kinetics, which results in reduced residual stresses while retaining the high strengths and hardnesses that are desirable for bearing applications.

This multimodal study will include rolling contact fatigue characterization, residual stress and hardness measurement and time/temperature/transformation studies of selected Ni-Ti-Hf alloys. Alloy optimization will be conducted by varying the nickel contents by 50.3 – 56.0 at. % and hafnium contents by 1.0 – 8.0 at. %. **Figure 17.2** outlines the optimized alloy design space of the project that shows varied nickel and hafnium contents. The sample compositions that have been tested in rolling contact fatigue are investigated via transmission electron microscopy (TEM) are highlighted in previous work [17.2] in addition to recent progress [17.3]. Likely outcomes to the study include further understanding of rolling contact fatigue performance, failure mechanisms, performance (hardness, strength, lifetime predictions) versus residual stresses, and a map of alloy design space to allow for optimization of Ni-Ti-Hf alloys for tribology applications.

17.2 Previous Work

17.2.1. Rolling Contact Fatigue

It is known that for nickel-rich compositions of Ni-Ti, and also ternary Ni-Ti-Hf compositions with low amounts of hafnium (~ 1 at. %), the Ni_4Ti_3 phase may be used for precipitation hardening without compromising the high hardness of the solid solution. In fact, the precipitates can also increase the hardness of the alloys. However, for Ni-Ti-Hf with greater amounts of Hf (8 at. % or more), Hf and Ni rich "H-phase" precipitates form instead of Ni_4Ti_3 and provide even greater strengthening. Therefore, it is hypothesized that H-phase precipitation can also provide superior hardness, resulting in superior wear performance in alloys under rolling contact fatigue (RCF) conditions. Testing of Ni-Ti-Hf samples using a three ball-on-rod set-up is imperative to ensuring this hardening behavior improves the component from an engineering standpoint.

A significant reduction in rolling contact fatigue performance has been observed in the $Ni_{54}Ti_{45}Hf_1$ alloy between 1.9 and 2.0 GPa. The brittle nature of spalling failures that are common in the specimens that failed at 2 GPa provide insight to the dominant failure mechanisms under Hertzian contact conditions [1]. Specifically, it was speculated that there must be a change in the uniaxial stress-strain behavior (for instance, the critical stress for martensite formation) in the range of 1.9-2.0 GPa that can be related to rolling contact fatigue performance. Thus, uniaxial compression testing on the same material as tested under RCF conditions was conducted to provide insight into the relationship between the critical contact stresses under fatigue conditions and the distinctive features on the stress-strain curves.

17.2.2. TEM Characterization

NiTiHf alloys with target compositions of $Ni_{56}Ti_{41}Hf_3$ and $Ni_{56}Ti_{36}Hf_8$ were made by induction-melting high-purity elemental constituents using a graphite crucible and casting into a copper mold. The ingots were homogenized in vacuum at 1050ºC for 72 h and then extruded at 900ºC at a 7:1 area reduction ratio. The extruded rods were sectioned into samples that were initially solution annealed at 1050ºC for 30 minutes and water quenched. Samples of each composition were then pre-aged at 300 ºC for 12 h and air cooled, and finally aged a second time at 500 ºC for 4 h and air-cooled. To isolate the effect of pre-aging on the functional properties of Ni-Ti-Hf alloys, other test samples were directly aged at 550ºC for 4 h after the solution-anneal treatment (without pre-aging at 300ºC for 12 h). Conventional and high-resolution transmission electron microscopy (HR-TEM), bright-field transmission electron microscopy and selected area electron diffraction microscopy of aged Ni-Ti-Hf samples was carried out using an FEI Talos TEM (FEG, 200 kV). The TEM foils were prepared by electro-polishing in an electrolyte of 30% HNO_3 in methanol (by volume) at around −35ºC. To measure the average size and spacing of the H-phase and Ni_4Ti_3 precipitates in addition to observing precipitate morphology, several HRTEM taken from various regions were analyzed. A probe-corrected FEI Titan 1 was employed to take atomic resolution scanning transmission electron microscopy (HR-STEM) images of some of the microstructures. Digital Micrograph was utilized to extract diffraction information of the precipitates analyzed in the collected HRTEM and HR-STEM images.

Findings through these techniques indicate a significant change in microstructure and properties by adjustments in composition and secondary thermal processing. The effect of Hf addition shows a direct change in preference from one secondary precipitation type. In **Fig. 17.3** Ni_4Ti_3 readily forms after solution anneal and water quench and in **Fig. 17.4** H-phase slowly begins to nucleate and grow. In the $Ni_{56}Ti_{36}Hf_8$ alloy, preference for fine H-phase precipitation resulted in higher toughness [2]. In the $Ni_{56}Ti_{41}Hf_3$ alloy, preference for equiaxed Ni_4Ti_3 precipitation resulted in higher toughness [3,4]. The effect of secondary processing via multi-step heat treatments show a change in the precipitates formed in a given sample. A two-step heat treatment of solution heat treatment and water quenching, and then a secondary aging step at 550ºC before air-cooling reveals only one precipitate type.

17.3 Recent Progress

17.3.1. Rolling Contact Fatigue of peak-aged NiTi and NiTiHf alloys

RCF testing was performed on 6 different alloys in their peak-aged conditions (**Table 17.1.**)and the contact stress vs. cycles to failure for each alloy is presented in **Fig. 17.5.** The baseline $Ni_{55}Ti_{45}$ alloy (blue) was initially tested and compared with the 1st generation $Ni_{54}Ti_{45}Hf_1$ alloy (red), both of which exhibited failures at a threshold contact stress level of ~1.9 GPa which is in alignment with their similar hardness (677 and 688 HV). $Ni_{50.3}Ti_{46.7}Hf_3$ alloy has the lowest Ni and Hf levels of the 2nd generation alloys and has comparable hardness (692 HV) with $Ni_{55}Ti_{45}$ and $Ni_{54}Ti_{45}Hf_1$. This alloy performed well at more modest stress levels (~1.7 GPa) but, as with the baseline and 1st generation alloys, it began experiencing failures at ~1.9 GPa. RCF performance evaluation of the high Ni and Hf compositions (54–56 at. % Ni, 3–8 at. % Hf) was conducted for $Ni_{54}Ti_{43}Hf_3$, $Ni_{56}Ti_{41}Hf_3$, and $Ni_{56}Ti_{36}Hf_8$ alloys and, clearly their increased hardness (735–769 HV) results in a notable RCF performance. Although these compositions began to fail at stress levels of 2.0–2.1 GPa, the $Ni_{56}Ti_{36}Hf_8$ and $Ni_{56}Ti_{41}Hf_3$ alloys still exhibited runouts at 2.1 GPa. Furthermore, many of the tests on the very hard (above 700 HV) NiTiHf alloys still achieved long life-spans ~10^7 cycles at 2.1 GPa, even though they were not deemed runouts. This type of failure after extensive cyclic is a result of high-cycle fatigue. Comparatively, the lower hardness alloys (below 700 HV) tended to fail well before this due to overloading of the material. It is clear that hardness plays an important role in the longevity of RCF tests and that by implementing novel peak-aging heat treatments oil-lubricated RCF performance is enhanced.

17.3.2. TEM Characterization of peak-aged NiTi and NiTiHf Alloys

Fig. 17.6. shows BF-TEM micrographs of 6 alloys at the peak-aged conditions (**Table 17.1.**) before deformation. Binary $Ni_{55}Ti_{45}$ contains 51 % area fraction of nano-scale Ni_4Ti_3 precipitates (31 ± 6 nm) within B2 matrix (**Fig. 17.6(a))** which is the most important precipitation hardening component in Ni-rich NiTi-based alloys [4,5]. The baseline alloy also contains large (~1.3 μm) Ni_3Ti phase (detected by spot EDX in TEM mode) which typically form on grain boundaries. $Ti_2Ni(O)$ oxides (~800 nm) were also observed in this alloy. These phases are detrimental to strength and fatigue performance [4–6]. The 1st generation $Ni_{54}Ti_{45}Hf_1$ alloy achieved a similar hardness to the baseline alloy as well as similar RCF performance. The microstructure contains 54 % area fraction of nano-scale Ni_4Ti_3 precipitates (27 ± 9 nm) within the matrix (**Fig. 17.6(b)**) which has not changed much compared to the baseline alloy. Unlike the baseline alloy, however, the 1 at. % Hf addition prevented the formation of heterogeneous Ni_3Ti phase after aging [2]. The peak-aged $Ni_{50.3}Ti_{46.7}Hf_3$ alloy shows a slightly higher hardness (692 HV) compared with the baseline and 1st generation alloys. Despite the lower Ni content in this alloy, the slight increase in hardness is attributed to dense precipitation (**Fig. 17.6(c))** of 37 % area fraction of Ni_4Ti_3 (25 ± 8 nm) precipitates and 22 % area fraction of H-phase precipitates (32 ± 13 nm (l), 14 ± 5 nm (w)) with a low area fraction of B2 matrix (41 %) compared with the baseline and 1st generation alloys.

When the Ni content is increased in $Ni_{54}Ti_{43}Hf_3$ alloy, both the hardness (735 HV) and RCF performance is improved compared with the previous three alloys. It is clear from **Fig. 17.6(d)**, this behavior is attributed to the high density (67 %) of Ni_4Ti_3 precipitates (74 ± 11 nm). It is worth mentioning the change in Ni_4Ti_3 morphology from the common lens-shaped in binary NiTi alloys to equiaxed-shaped is related to reduced lattice mismatch between the precipitates and the matrix [7] in the direction normal to the habit plane which results in growth in both directions (normal and parallel to habit plane) [7–9]. When the Ni-content is increased in the $Ni_{56}Ti_{41}Hf_3$ alloy (**Fig. 17.6(e)**), the hardness further increases to 752 HV and the RCF performance is improved (runout at 2.1 GPa). This improvement is attributed to higher fraction (71 %) of equiaxed Ni_4Ti_3 precipitates (81 ± 15 nm). Moreover, low-temperature pre-aging has shown to be more effective over conventional higher temperature heat treatments (400–700ºC) for the $Ni_{54}Ti_{43}Hf_3$ and $Ni_{56}Ti_{41}Hf_3$ alloys resulting in controlled Ni_4Ti_3 precipitate growth [5,10]. The $Ni_{56}Ti_{36}Hf_8$ alloy (**Fig. 17.6(f)**) achieved the highest hardness and consequently showed the best RCF performance of all examined alloys. Changes in Hf and Ni alloy content combined with 3-step aging treatment allows for a unique microstructure containing 33 % area fraction of dense $Ni_{16}Ti_{11}$ (16 ± 5 nm (l), 11 ± 7 nm (w)) combined with 61 % area fraction of H-phase (23 ± 5 nm (l), 12 ± 3 nm (w)) precipitates results in the lowest fraction of B2 matrix (13 %) constraining this softer phase to narrow (5 nm) channels. The novel cubic structured $Ni_{16}Ti_{11}$ precipitates has been the focus of recent investigation by Mills et al. [11]. Moreover, the calculated hardness of $Ni_{16}Ti_{11}$ is shown to be higher than B2 and H-phase which explains the high alloy hardness and ideal properties for wear-resistant bearing components. Additional contribution to the hardness in all of the alloys is connected to solid-solution strengthening component from excess Ni and Hf atoms within the matrix [12]. **Table 17.2** summarizes the statistical measurements made for the 6 alloy microstructures, such as precipitate size (nm) and area fraction (%).

17.4 Plans for Next Reporting Period

Finalize deformation RCF paper manuscript, finalize PhD thesis, and defend Thesis October 28th.

17.5 References

[17.1] C. Della Corte, M.K. Stanford, T.R. Jett, Rolling contact fatigue of superelastic intermetallic materials (SIM) for Use as resilient corrosion resistant bearings, Tribol. Lett. 57 (2015) 1–10.

[17.2] B. Hornbuckle, R. Noebe, G. Thompson, Influence of Hf solute additions on the precipitation and hardenability in Ni-rich NiTi alloys, J. Alloys Compd. 640 (2015) 449–454.

[17.3] K. Otsuka, X. Ren, Physical metallurgy of Ti–Ni-based shape memory alloys, Prog. Mater. Sci. 50 (2005) 511–678.

[17.4] O. Benafan, A. Garg, R. Noebe, H. Skorpenske, K. An, N. Schell, Deformation characteristics of the intermetallic alloy 60NiTi, Intermetallics. 82 (2017) 40–52.

[17.5] B.C. Hornbuckle, X.Y. Xiao, R.D. Noebe, R. Martens, M.L. Weaver, G.B. Thompson, Hardening behavior and phase decomposition in very Ni-rich Nitinol alloys, Mater. Sci. Eng. A. 639 (2015) 336–344.

[17.6] Q. Qin, H. Peng, Q. Fan, L. Zhang, Y. Wen, Effect of second phase precipitation on martensitic transformation and hardness in highly Ni-rich NiTi alloys, J. Alloys Compd. 739 (2018) 873–881.

[17.7] S. Mills, A.P. Stebner, M.J. Mills, C. Della Corte, R.D. Noebe, B. Amin-Ahmadi, Characterization of Ni-rich NiTiHf Alloys for Tribology Applications Using Advanced TEM Techniques, ArXiv. (n.d.). www.arxiv.org.

[17.8] F. Zhang, L. Zheng, F. Wang, H. Zhang, Effects of Nb additions on the precipitate morphology and hardening behavior of Ni-rich Ni 55 Ti 45 alloys, J. Alloys Compd. 735 (2018) 2453–2461.

[17.9] W. Tirry, D. Schryvers, High resolution TEM study of Ni4Ti3 precipitates in austenitic Ni51Ti49, Mater. Sci. Eng. A. 378 (2004) 157–160.

[17.10] M. Moshref-Javadi, S.H. Seyedein, M.T. Salehi, M.R. Aboutalebi, Age-induced multi-stage transformation in a Ni-rich NiTiHf alloy, Acta Mater. 61 (2013) 2583–2594.

[17.11] S. Mills, Y. Hong, M. Alse-Zaeem, C. Dellacorte, R.D. Noebe, A.P. Stebner, B. Amin-Ahmadi, Identification of a Ni16Ti11 precipitate phase within nickel-rich, nickel-titanium-based alloys, ArXiv. (n.d.). www.arXiv.org.

[17.12] L. Gypen, Ajj. Deruyttere, Multi-component solid solution hardening, J. Mater. Sci. 12 (1977) 1028–1033.

[17.13] L. Casalena, A.N. Bucsek, D.C. Pagan, G.M. Hommer, G.S. Bigelow, M. Obstalecki, R.D. Noebe, M.J. Mills, A.P. Stebner, Structure-Property Relationships of a High Strength Superelastic NiTi–1Hf Alloy, Adv. Eng. Mater. 20 (2018) 1800046.

17.6 Figures and Tables

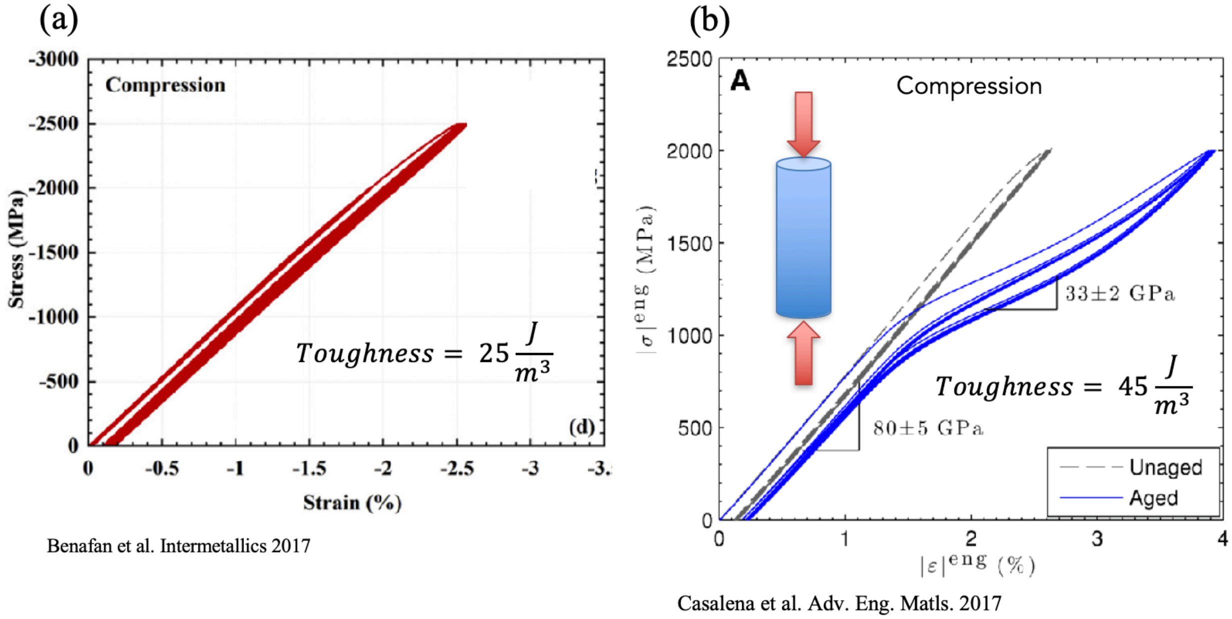

Figure 17.1: (a) 5-cycle compressive response of intermetallic $Ni_{55}Ti_{45}$ shows no super-elasticity [4]. (b) 5-cycle compressive response of $Ni_{54}Ti_{45}Hf_1$ shows super-elasticity with little to no hysteresis [13]. As a result, nearly doubled toughness in the ternary alloy compared to the binary alloy.

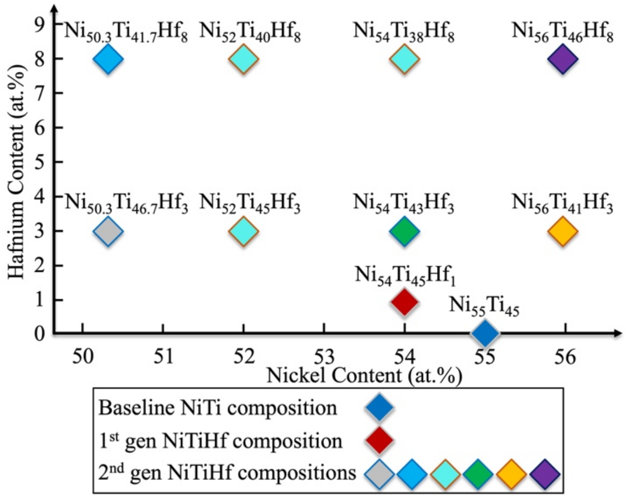

Figure 17.2: Target composition space of Ni-rich NiTiHf alloys developed for tribological applications which are compared against $Ni_{55}Ti_{45}$ and $Ni_{54}Ti_{45}Hf_1$ baseline alloys.

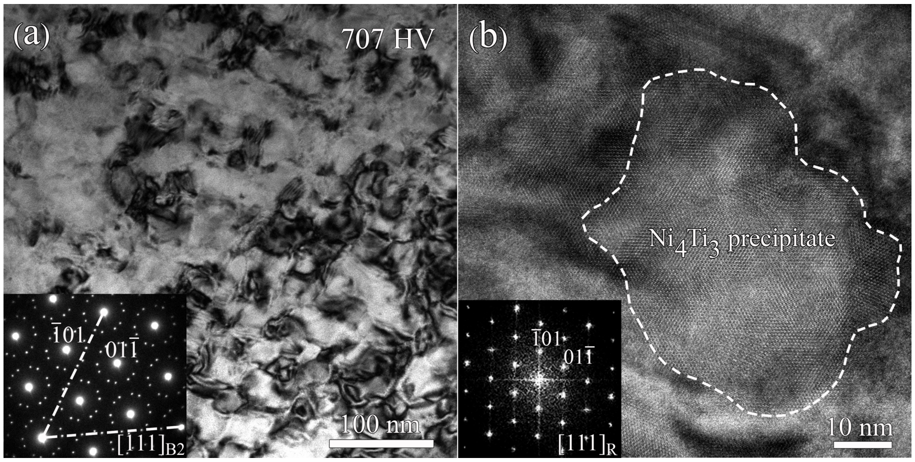

Figure 17.3: (a) Conventional BF-TEM micrograph of $Ni_{56}Ti_{41}Hf_3$ after solution annealing at 1050 °C for 0.5 h. Corresponding SAED pattern in the bottom left inset taken along $[111]_{B2}$ zone axis showing the super reflections originated from two variants of Ni_4Ti_3 precipitates. (b) HRTEM micrograph taken along $([111]_R//[111]_{B2})$ showing a monolithic Ni_4Ti_3 precipitate within B2 matrix.

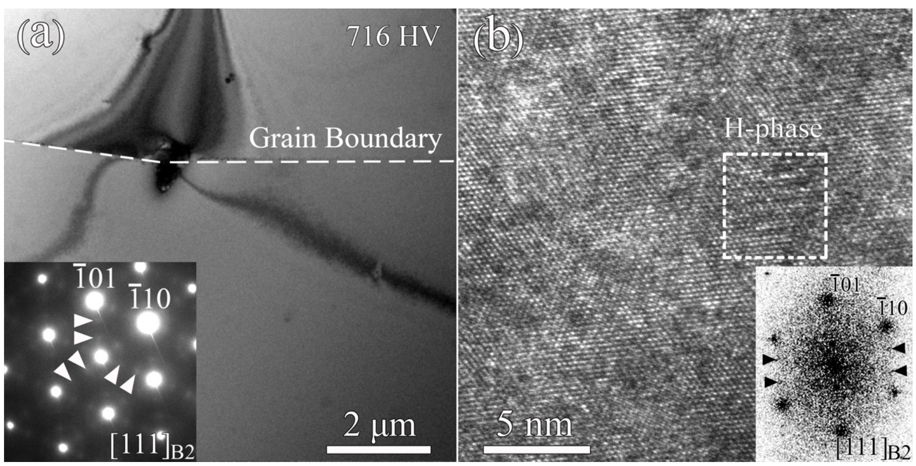

Figure 17.4: (a) BF-TEM micrograph of $Ni_{56}Ti_{36}Hf_8$ after solution annealing at 1050 °C for 0.5 h. Corresponding SAED pattern in the bottom left inset are taken along $[111]_{B2}$ showing the weak super reflections originated from 3 different variants of H-phase precipitates along 1/3<011> (indicated by arrowheads). (b) HRTEM micrograph taken along $[111]_{B2}$ showing a small H-phase precipitate. The super reflections originated from the H-phase precipitate are indicated by arrowheads in the FFT pattern.

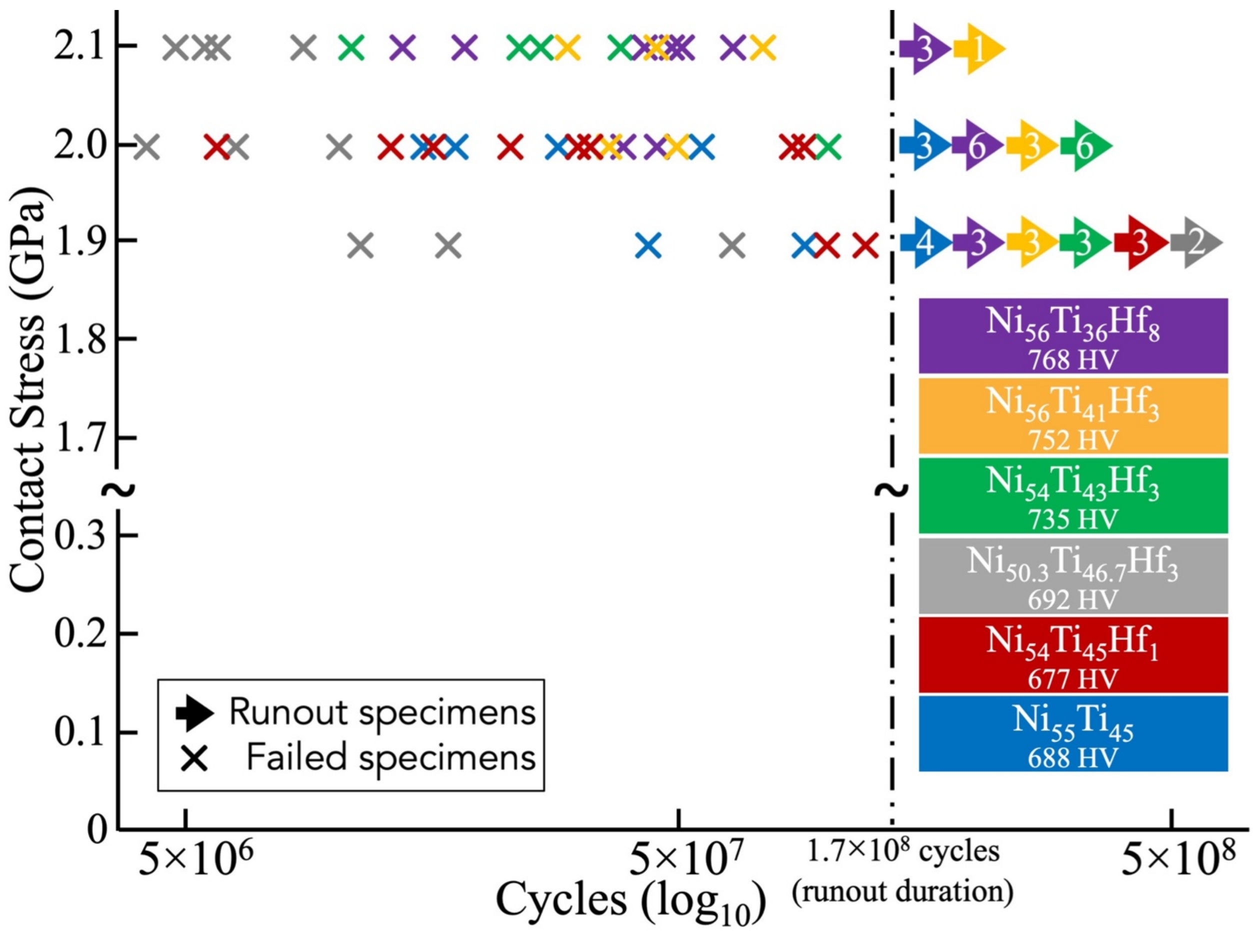

Figure 17.5: RCF test results of Ni-rich NiTiHf alloys at peak-aged conditions (Table 17.X) indicating Hertzian contact stress (GPa) vs. cycles to failure ($\log_{10}$). Vertical dashed black line indicates runout condition where tests that did not fail for the specific duration were manually shut off. Runout conditions are labeled to the right of the line (arrows). Tests that failed prior to the runout condition are shown to the left of the dotted line.

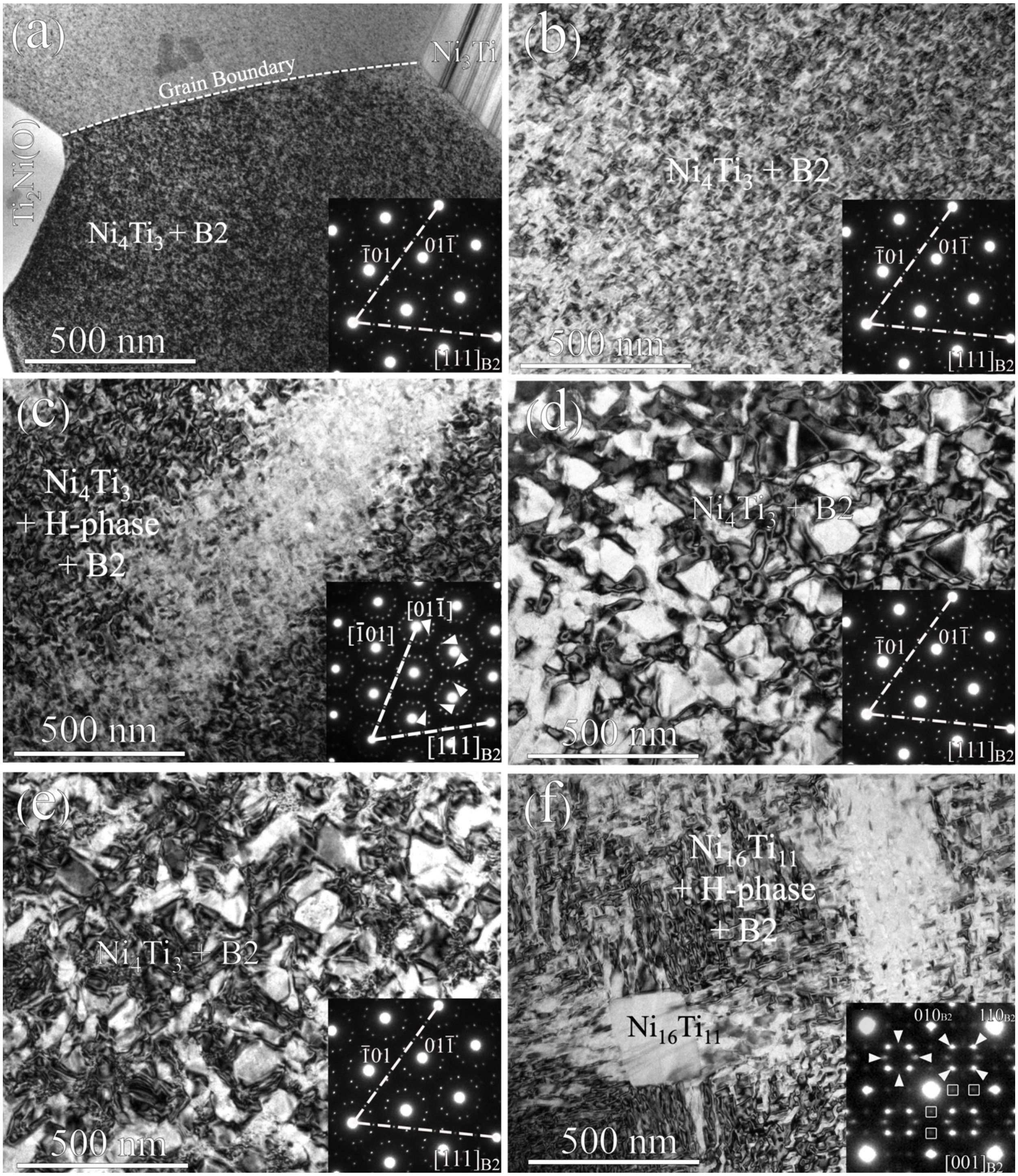

Figure 17.6: (a) Baseline NiTi alloy contains nano-scale Ni_4Ti_3 and heterogeneous Ni_3Ti and $Ti_2Ni(O)$. (b) 1st generation $Ni_{54}Ti_{45}Hf_1$ alloy containing nano-scale Ni_4Ti_3. (c) $Ni_{50.3}Ti_{46.7}Hf_3$ alloy containing nano-scale Ni_4Ti_3 and H-phase. (d) $Ni_{54}Ti_{43}Hf_3$ alloy containing equiaxed Ni_4Ti_3. (e) $Ni_{56}Ti_{41}Hf_3$ alloy containing equiaxed Ni_4Ti_3. (f) $Ni_{56}Ti_{36}Hf_8$ alloy containing nano-scale $Ni_{16}Ti_{11}$ and H-phase. Rare larger $Ni_{16}Ti_{11}$ islands are also present.

Table 17.1: Hardness values of NiTi and NiTiHf alloys under peak-aged treatments

Composition (at. %)	Heat treatment	Hardness (HV)
$Ni_{56}Ti_{36}Hf_{8}$	SA_{WQ} + 300ºC (12 h) + 550ºC (4 h)	769
$Ni_{54}Ti_{38}Hf_{8}$	SA_{WQ} + 300ºC (12 h) + 550ºC (4 h)	742
$Ni_{52}Ti_{40}Hf_{8}$	SA_{WQ} + 300ºC (12 h) + 400ºC (4 h)	712
$Ni_{50.3}Ti_{41.7}Hf_{8}$	SA_{WQ} + 300ºC (12 h) + 400ºC (4 h)	639
$Ni_{56}Ti_{41}Hf_{3}$	SA_{WQ} + 300ºC (12 h)	752
$Ni_{54}Ti_{43}Hf_{3}$	SA_{WQ} + 300ºC (12 h)	735
$Ni_{52}Ti_{45}Hf_{3}$	SA_{WQ} + 300ºC (12 h) + 400ºC (1.5 h)	705
$Ni_{50.3}Ti_{46.7}Hf_{3}$	SA_{WQ} + 300ºC (12 h) + 400ºC (1.5 h)	692
$Ni_{54}Ti_{45}Hf_{1}$	SA_{WQ} + 400ºC (.5 h)	677
$Ni_{55}Ti_{45}$	SA_{WQ} + 400ºC (1 h)	688

Table 17.2: Statistical measurements of peak-aged NiTi and NiTiHf alloys

Composition	Ni_4Ti_3 size (nm)	Ni_4Ti_3 fraction (%)	H-phase size (nm)	H-phase fraction (%)	$Ni_{16}Ti_{11}$ size (nm)	$Ni_{16}Ti_{11}$ fraction (%)
$Ni_{55}Ti_{45}$	31 ± 6	51	– –	– –	– –	– –
$Ni_{54}Ti_{45}Hf_{1}$	27 ± 9	54	– –	– –	– –	– –
$Ni_{50.3}Ti_{46.7}Hf_{3}$	25 ± 8	37	32 ± 13 (l), 14 ± 5 (w)	22	– –	– –
$Ni_{54}Ti_{43}Hf_{3}$	74 ± 11	67	– –	– –	– –	– –
$Ni_{56}Ti_{41}Hf_{3}$	81 ± 15	71	– –	– –	– –	– –
$Ni_{56}Ti_{36}Hf_{8}$			23 ± 5 (l), 12 ± 3 (w)	61	16 ± 5 (l), 11 ± 7 (w)	33